Proc. Natl. Acad. Sci. USA
Vol. 93, pp. 5357–5362, May 1996
Biochemistry

Three-dimensional structure of human protein kinase C interacting protein 1, a member of the HIT family of proteins

(signal transduction/SIRAS/histidine triad)

CHRISTOPHER D. LIMA*, MICHAEL G. KLEIN†, I. BERNARD WEINSTEIN†, AND WAYNE A. HENDRICKSON*‡

*Department of Biochemistry and Molecular Biophysics and ‡Howard Hughes Medical Institute, Columbia University, New York, NY 10032; and †Columbia–Presbyterian Cancer Center and Institute of Human Nutrition, New York, NY 10032

Contributed by Wayne A. Hendrickson, January 22, 1996

ABSTRACT **The three-dimensional structure of protein kinase C interacting protein 1 (PKCI-1) has been solved to high resolution by x-ray crystallography using single isomorphous replacement with anomalous scattering. The gene encoding human PKCI-1 was cloned from a cDNA library by using a partial sequence obtained from interactions identified in the yeast two-hybrid system between PKCI-1 and the regulatory domain of protein kinase C-β. The PKCI-1 protein was expressed in *Pichia pastoris* as a dimer of two 13.7-kDa polypeptides. PKCI-1 is a member of the HIT family of proteins, shown by sequence identity to be conserved in a broad range of organisms including mycoplasma, plants, and humans. Despite the ubiquity of this protein sequence in nature, no distinct function has been shown for the protein product *in vitro* or *in vivo*. The PKCI-1 protomer has an α+β meander fold containing a five-stranded antiparallel sheet and two helices. Two protomers come together to form a 10-stranded antiparallel sheet with extensive contacts between a helix and carboxy terminal amino acids of a protomer with the corresponding amino acids in the other protomer. PKCI-1 has been shown to interact specifically with zinc. The three-dimensional structure has been solved in the presence and absence of zinc and in two crystal forms. The structure of human PKCI-1 provides a model of this family of proteins which suggests a stable fold conserved throughout nature.**

A protein kinase C (PKC) inhibitory protein designated PKCI-1 (for PKC interacting protein 1) was initially purified from bovine brain as a potent inhibitor of protein kinase C (1–4). Since that time, other investigators have characterized a protein similar to bovine PKCI-1 from other organisms and have not been able to demonstrate inhibitory effect on PKC activity (ref. 5; M.G.K. and C.D.L., unpublished observations). In addition, some doubt has been cast on the physiological relevance of PKC inhibition by bovine PKCI-1 (6). Because of subsequent results obtained in the yeast two-hybrid system (described below), we have designated this protein PKC interacting protein, employing the same acronym PKCI-1.

PKCI-1 has been shown to interact with the regulatory domain of PKC-β in the yeast two-hybrid system (M.G.K., unpublished observations). PKCI-1 has also been shown to interact with the ataxia-telangiectasia group D (ATDC) protein in the yeast two-hybrid system (7). The ATDC protein is implicated in the human genetic disease ataxia-telangiectasia. In addition, an open reading frame (ORF) encoding a cyanobacterial PKCI-1 homologue has been identified, and inactivation of this ORF in cyanobacteria results in a slow growth phenotype for this organism (8). These results suggest a possible role for PKCI-1 in signal transduction pathways.

Several DNA ORFs coding for a protein similar to bovine PKCI-1 have been identified in a broad range of organisms including mycoplasma, plants, and humans (9, 10). Some have been grouped into the HIT protein family and into a novel class of zinc-binding proteins. The acronym HIT refers to a conserved triad of histidines that is thought to interact with zinc.

PKCI-1 from bovine brain and maize were purified as heat stable proteins and shown to specifically bind zinc (1–3, 5, 11). The zinc-binding motif of PKCI-1 was initially identified by synthesizing peptides from various regions of PKCI-1 and demonstrating their ability to specifically bind zinc. A histidine-rich peptide (His-Val-His-Leu-His) near the carboxy terminal end of the polypeptide was identified as having the ability to bind zinc in the micromolar range. In addition, the His-Xaa-His-Xaa-His motif is almost completely conserved throughout this family of proteins.

Zinc and metal free (apo) forms of human PKCI-1 have been crystallized and solved to high resolution using x-ray crystallographic methods. Structural and sequence analyses have identified elements of these structures that are conserved throughout a broad range of organisms. The presumed structural similarities of PKCI-1 between organisms has implications with respect to the mechanism of zinc binding and for the potential surfaces of the molecule which may be involved in protein/protein interactions and the *in vivo* functions of PKCI-1.

MATERIALS AND METHODS

Cloning. A human PKCI-1 cDNA sequence was identified by using the yeast two-hybrid system during studies designed to isolate proteins that interact with the regulatory domain of PKC-β. The yeast two-hybrid screen was conducted by using a fusion between LexA and the amino-terminal 317 amino acids of PKC-β (12) as a probe. By screening 300,000 colonies expressing a HL-60 cDNA library fused to the Gal4 activation domain (13), we identified a single colony that activated the LacZ reporter gene only in the presence of the bait plasmid but was unable to activate LacZ expression when tested using LexA alone. This clone was identified by sequence alignment with bovine PKCI-1 as a partial human PKCI-1 cDNA lacking the amino-terminal 31 amino acids, such that the Gal4 activation domain was fused to the sequence encoding isoleucine 32 of human PKCI-1. The entire PKCI-1 cDNA coding sequence was obtained from a HL-60 Zap library (Stratagene) by hybridization to a polymerase chain reaction (PCR) generated probe (14), which amplified sequences of human PKCI-1 encoding amino acids 36–54.

Antibodies. Polyclonal antibodies were generated against a bacterially expressed glutathione-*S*-transferase (GST)/PKCI-1 fusion protein by injecting the factor Xa cleaved-PKCI-1 component of the fusion protein into rabbits. The antiserum was affinity purified by passing it over a cyanogen bromide-activated sepharose column to which the GST/PKCI-1 fusion protein was

The publication costs of this article were defrayed in part by page charge payment. This article must therefore be hereby marked "*advertisement*" in accordance with 18 U.S.C. §1734 solely to indicate this fact.

Abbreviations: PKC, protein kinase C; PCKI-1, PKC interacting protein 1; ORF, open reading frame; 2-ME, 2-mercaptoethanol.

Data deposition: The sequence reported in this paper has been deposited in the GenBank data base (accession no. U51004).
Data deposition: The atomic coordinates and structure factors have been deposited in the Protein Data Bank, Chemistry Department, Brookhaven National Laboratory, Upton, NY 11973 (references 1kpa, 1kpb, 1kpc). This information is available immediately.

covalently coupled. Western blot analysis of several cell types indicated that the antibody raised against bacterially expressed PKCI-1 detected a 14-kDa band, which is consistent with the expected molecular weight of PKCI-1. PKCI-1 was detected in several human tumor cell lines including breast, esophageal and colon cancer cells, promyelocytic leukemia cells (HL-60), and HeLa cells. This antibody also detected a protein of the expected molecular weight in primary human skin fibroblasts, mouse NIH 3T3 fibroblasts, rat 6 fibroblasts, K22 rat liver epithelial cells, bovine aortic endothelial cells, HC11 mouse mammary epithelial cells, rat intestinal epithelial cells, IEC18, and several other cell lines (data not shown). Other studies (2, 5) have shown that PKCI-1 is present in a wide variety of tissues, indicating that it is expressed across a broad range of species and tissue.

Expression and Purification. The human PKCI-1 cDNA was subcloned into pHIL-D5, a vector for use in the yeast *Pichia pastoris* overexpression system (Invitrogen). It was hoped that certain isoforms of PKC might be stabilized in this overexpression system by forming a complex with PKCI-1. Therefore, several PKC isoforms were cloned into this vector with restriction sites engineered either 5′ or 3′ of the ORF of the PKC isoform of interest. The plasmid was constructed so the preceding ORF would include a termination codon, a frame shift, and the start codon of the subsequent ORF. In this way, it was hoped that a mRNA chimera would produce both the PKC isotype of interest and the PKCI-1 gene product in equamolar amounts. Although active forms of PKC were expressed in this system, no PKC–PKCI-1 complexes were observed in extracts of these cells (C.D.L., unpublished observations).

A MUT-strain of *P. pastoris* carrrying the pHIL-D5 genomic insertion containing human PKCI-1 and PKC-α cDNA sequences was grown in minimal media in 1.5-liter flasks in 12-liter batches for 2 to 3 days or until the culture reached saturation. The culture was centrifuged and the pellet resuspended in 25% of the original volume in minimal medium containing 0.5% methanol, and grown for an additional 2 days. The cells were again centrifuged and resuspended in a buffer containing 20 mM Tris (pH 8.0), 10 mM 2-mercaptoethanol (2-ME), 1 mM phenylmethylsulfonyl flouride, 1 mM EDTA, 0.1 mM pepstatin, and 20% sucrose. The cell suspension was placed into a bead beater (Biospec Products, Bartlesville, OK) and lysed using eight 30-sec pulses. The lysate was cleared by centrifugation and dialyzed against 20 mM Tris (pH 8.0), 1 mM EDTA, 5 mM 2-ME, and 0.1 mM phenylmethylsulfonyl flouride (buffer A). The lysate was loaded onto a Q sepharose 26/10 column (Pharmacia) for batch elution. A 100 mM NaCl batch elution in buffer A eluted PKCI-1 from this column. PKCI-1 could be visualized in the crude lysate and through purification by SDS/PAGE. The fraction containing PKCI-1 was dialyzed against buffer A and placed onto a Mono Q 10/10 column and eluted using a 200 ml gradient from 0 to 80 mM NaCl in buffer A. The fractions containing PKCI-1 were concentrated and loaded onto a Hiload 26/60 Superdex 200 column (Pharmacia) in buffer A. The protein eluted as a dimer from this column and was reapplied to the Mono Q 10/10 column and eluted with a gradient of 0 to 80 mM NaCl. This protocol yielded 2–3 mg of >95% pure apo-PKCI-1 (without zinc) as analyzed by SDS/PAGE. The protocol was modified to purify zinc-PKCI-1 by substituting 50 μM zinc acetate for 1 mM EDTA in buffer A throughout the purification. Both preparations could be stored at −80°C after flash freezing. Zinc–PKCI-1 had to be stored at 0.5 mg/ml to prevent aggregation. Apo-PKCI-1 could be stored at or above 10 mg/ml. In both instances, the final storage buffer included 5 mM Tris (pH 7.5) and 1 mM 2-ME.

Crystallization. Microcrystals of apo-PKCI-1 were obtained using a partial factorial screen (ref. 15; Hampton Research). Final conditions that yielded single crystals included 13–18% PEG 8000 and 100 mM sodium cacodylate pH 6.5 at 20°C. Crystallizations were set up using 10 mg of apo-PKCI-1 per ml and 3–6 mg of zinc–PKCI-1 per ml. Zinc–PKCI-1 is concentrated just before the protein is set up for crystallization. Hanging drops containing the zinc–PKCI-1 precipitated immediately upon addition of the well solution. Crystals nucleated from the dense precipitate and as they grew, they slowly dissolved the precipitate around them. In several cases this occurred until all of the precipitate redissolved and the drop contained only crystalline material. In contrast, hanging drops containing apo-PKCI-1 remained clear until crystals appeared in the drops.

Crystals of apo-PKCI-1 occurred in two space groups, $P2_1$ with unit cell constants of a = 63.9 Å, b = 78.7 Å, c = 46.3 Å, β = 90°, and $P2_12_12_1$ with unit cell constants of a = 46.1 Å, b = 77.3 Å, c = 81.0 Å. Apo-PKCI-1 primarily crystallized in space group $P2_1$ and only after several months did crystals of space group $P2_12_12_1$ appear, and then just in a couple of instances. Zinc–PKCI-1 only crystallized in space group $P2_12_12_1$. The $P2_1$ crystal has pseudo $P2_12_12$ symmetry and ranges in degree of its false symmetry from crystal to crystal.

Data Collection and Structure Determination. Four data sets were collected and used to solve and analyze the structure of PKCI-1. These included a data set collected on a zinc–PKCI-1 $P2_12_12_1$ crystal, an apo-PKCI-1 $P2_12_12_1$ crystal, an apo-PKCI-1 $P2_1$ crystal into which 0.1 mM zinc acetate had been soaked, and a zinc–PKCI-1 $P2_12_12_1$ crystal derivatized with $Hg(CN)_2$. Single isomorphous replacement with anomalous scattering (SIRAS) phases were calculated and interpretable electron density was generated using the zinc $P2_12_12_1$ and mercurated zinc $P2_12_12_1$ data sets (Table 1, Fig. 1). The current R value for the zinc–PKCI-1 model in space group $P2_12_12_1$ is 19.2% and the free R is 26.1% from 10.0 to 2.0 Å. The apo-PKCI-1 model in space group $P2_12_12_1$ has a current R value from 10.0 to 2.0 Å of 18.7% with a free R of 24.8%. The model for apo-PKCI-1 in space group $P2_1$ into which 0.1 mM zinc acetate has been soaked and has a current R value of 21.7% and a free R of 30.9 from 7.0 to 2.2 Å. The three structures of PKCI-1 have no interpretable density for amino acids 1–13 although significant nonwater density could be observed in several of the maps for amino acids 10–13.

Amino Terminal Sequencing, Proteolysis, and Electrospray Mass Spectroscopy. Several methods were employed to determine the composition of the amino terminal residues in PKCI-1 due to the lack of interpretable electron density in all three models. Amino terminal sequencing was done on zinc and apo-PKCI-1. In both cases, no sequence information could be obtained due to a presumed blockage at the amino terminus by a posttranslational modification. Bovine PKCI-1 has been shown to be acetylated on the second amino acid (3). Stable fragments of PKCI-1 ≈1 kDa smaller than full length PKCI-1 were obtained after proteolysis by subtilisin or trypsin. Amino terminal sequencing of these fragments showed that cleavage had occurred after Gln-9 with subtilisin and Lys-7 with trypsin. To determine the composition of the full length protein, zinc–PKCI-1 was sent to the Howard Hughes Mass Spectrometer Facility for analysis by electrospray mass spectroscopy. The molecular weight of PKCI-1 was determined to be 13712.9 atomic mass units with a second peak at 13789.5 atomic mass units. The calculated molecular weight for PKCI-1 acetylated on amino acid 2 is 13712.6 atomic mass units. The second peak was determined to be a 2-ME adduct of the acetylated protein, a product seen previously by mass spectroscopy (22). The acetylation of human PKCI-1 in the *P. pastoris* yeast expression system demonstrates the ability of this system to mimic a higher eukaryote in its posttranslational modifications of this protein in the cell.

RESULTS AND DISCUSSION

Overall Folding. The folding topology of PKCI-1 exhibited in all three refined structures can be described as a general $\alpha+\beta$ type and further subclassed into an $\alpha+\beta$ meander fold (23) (Fig. 2). Each protomer contains a five-stranded antiparallel sheet and two helices. In a protomer, helix A (residues 18–24) packs on one side of its five-stranded antiparallel sheet and helix B (residues

Table 1. Data and refinement statistics

	Native (zinc–PKCl-1)	Native (apo-PKCl-1)	Native (apo-PKCl-1 + 0.1 mM zinc)	$Hg(CN)_2$ (zinc)
Temperature	110 K	110 K	110 K	110 K
Space group	$P2_12_12_1$	$P2_12_12_1$	$P2_1$	$P2_12_12_1$
Cell	46.11, 77.29, 81.03	45.95, 76.69, 80.83	63.94, 78.66, 46.31	46.13, 78.13, 81.12
	90.00, 90.00, 90.00	90.00, 90.00, 90.00	90.00, 90.00, 90.00	90.00, 90.00, 90.00
dMin/λ	2.0 Å/1.2824 Å	2.0 Å/1.2824 Å	1.8 Å/0.910 Å	1.9 Å/1.5418 Å
Detector	Fuji image plates	Fuji image plates	Fuji image plates	RAXIS-II
No. of unique/no. of total reflections	17,754/213,583	17,662/99,583	36,570/82,407	19,762/109,809
Data coverage, %	88.6	89.7	86.3	83.6
*R*sym*	5.1	4.2	5.8	8.3
Refinement				
Resolution	10–2 Å	10–2 Å	7–2.2 Å	
R‡	0.192	0.187	0.217	
R_{free}§	0.261	0.248	0.309	
No. of reflections	17,425	17,140	21,145	
No. of total atoms	1982	1985	3735	
No. of protein/no. of water	1748/234	1748/237	3441/294	
rms bonds/angles	0.012/1.768	0.013/1.698	0.018/1.970	
avg/rms B mc	19.55/4.13	14.09/4.14	11.01/5.06	
avg/rms B sc	21.71/5.28	16.10/5.24	12.65/6.38	
rmsd from ncs‡	0.332 Å²	0.321 Å²	0.323 Å²	

SIRAS analysis	
MFID†	35.0
No. of common reflections	12,700
Resolution range	50–2.25 Å
No. of sites	4
Phasing power¶	2.32
Rc‖	0.61
Mean FOM**	0.457

Statistics are listed for the four data sets used in the structure determination and analysis of PKCI-1. A multiwavelength anomalous diffraction (MAD) data set was collected to 2.0 Å using a zinc–PKCI-1 $P2_12_12_1$ crystal at 110 K in an attempt to utilize the anomalous signal of zinc to derive phases capable of phasing the protein electron density. These data were collected on Howard Hughes beamline X4A at Brookhaven National Laboratory. Analysis of the MAD data set indicates that no interpretable anomalous signal is present. Two other data sets were collected on an apo-PKCI-1 $P2_12_12_1$ crystal and an apo 0.1 mM zinc soaked $P2_1$ crystal at 110K. A data set complete to 2.2 Å was collected using a RAXIS-II and modified Supper mirrors at Columbia on a $P2_12_12_1$ zinc crystal at 110 K derivitized with 1 mM $Hg(CN)_2$ and analyzed against the peak wavelength from the $P2_12_12_1$ MAD data set. All data sets were processed using DENZO (16) with subsequent data reduction performed using the CCP4 program suite (17). Two mercury positions were immediately interpretable in difference Pattersons. SIR phases were calculated using MLPHARE and difference Fourier analysis revealed two additional mercury positions. SIRAS phases were calculated using the four positions and analysis of the resulting electron density maps showed that good experimental phases could be determined by this method. An inverse beam data set was collected to obtain a complete data set of Bijvoet pairs to high resolution. Phasing and interpretable electron density to 2.25 Å was obtained (Fig. 1) whereupon the initial model was traced within a day using the bones and lego options in O (Fig. 1) (18). Each monomer, there is a dimer in the asymmetric unit, was traced independently. All models were refined using X-PLOR (19) using the cross-validation test (20). Phase combination to 2.25 Å with partial model and experimental SIRAS phases was used until all ordered amino acids were positioned. Refinement was extended to 2.0 Å whereupon water molecules were added. NCS restraints were not used with the dimer at any time during refinement. A data set was collected on an apo-PKCI-1 $P2_12_12_1$ crystal at beamline X4A to 2.0 Å. A partial zinc–PKCI-1 model was used between 10 and 2.5 Å in rigid body refinement against the apo data with an initial *R* value of 32.1%. Refinement was completed using 2Fo-Fc, Fo-Fc maps with model phases, and subsequently extended to 2.0 Å with no NCS restraints. A molecular replacement solution using AMORE (21) was found for the $P2_1$ data using the zinc–PKCI-1 structure as the search model between 8 and 3 Å. This solution was initially accomplished with the $P2_1$ data reduced in spacegroup $P2_12_12$. The *R* value for this solution is 44% with a correlation of 37 although when refined in X-PLOR, the *R* value does not drop below 30% and the free *R* remains high. When a self-rotation of this data reduced in space group *P*1 was analyzed, it is observed that the pseudo 2_1 axis and 2-fold axis origin peaks differed in height from the true 2_1 axis origin peak. A molecular replacement solution was determined using two search models, now two dimers in the asymmetric unit, with a fitted *R* value from AMORE of 33% with a correlation coefficient of 70 from 8 to 3 Å. The model was refined with no NCS restraints. All models underwent one round of simulated annealing in X-PLOR with positional refinement being used for all subsequent rounds. Weights on x-ray terms in all refinements were chosen to be less or equal to half the value suggested by X-PLOR.

*$R_{sym} = \Sigma|I - \langle I\rangle|/\Sigma I$, where I = observed intensity, and $\langle I\rangle$ = average intensity.

†MFID (mean fractional isomorphous difference) = $\Sigma||Fph| - Fp||/\Sigma|Fp|$, where Fp = protein structure factor amplitude and $|Fph|$ = heavy-atom derivative structure factor amplitude.

‡*R*, *R* based on 95% of the data used in refinement.

§R_{free}, *R* based on 5% of the data withheld for the cross-validation test.

¶Phasing power = root-mean-square ($|Fh|/E$), where $|Fh|$ = heavy-atom structure factor amplitude and E = residual lack of closure error.

‖$Rc = \Sigma||Fh(obs)| - |Fh(calc)||/\Sigma|Fh\ (obs)|$ for centric reflections where $|Fh(obs)|$ = observed heavy atom structure factor amplitude, and $|Fh(calc)|$ = calculated heavy-atom structure factor amplitude.

**Mean FOM = figure of merit.

††Least squares fitted rms deviations (rmsd) from noncrystallographic symmetry (ncs) between protomers in the asymmetric unit.

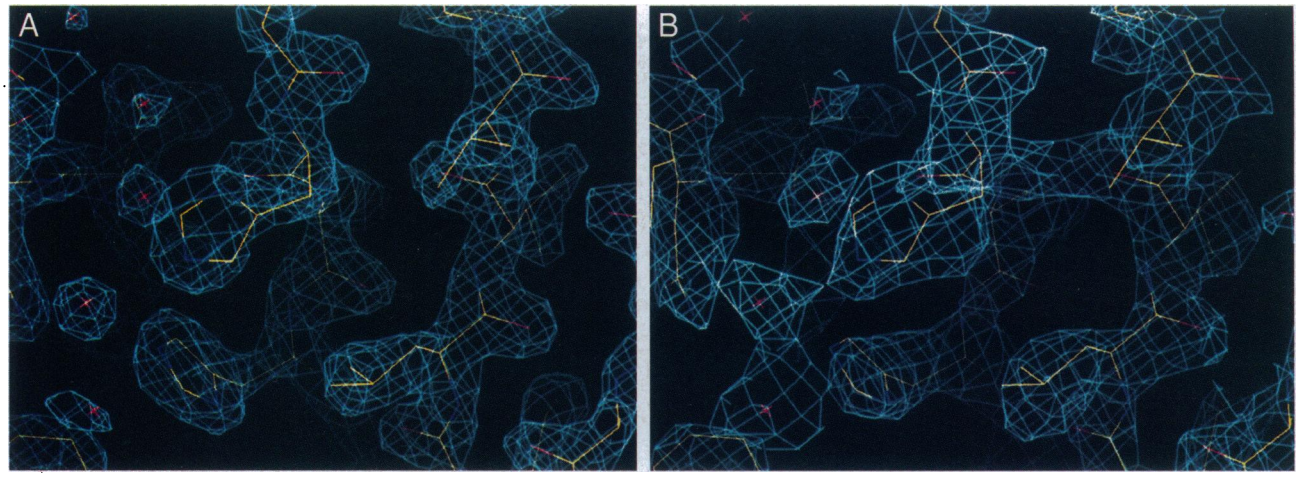

FIG. 1. Electron density for an exposed surface of PKCI-1 for zinc–PKCI-1. (*A*) Experimental electron density generated using SIRAS phases to 2.25 Å contoured at 1.25 σ for the region around the conserved histidines 112 and 114. (*B*) 2Fo-Fc electron density generated from the refined model showing the same region at 2.0 Å.

68–86) packs on the opposite side of the sheet. Two protomers are brought together in the dimer to form a 10-stranded antiparallel sheet, such that helix B from one protomer packs against helix B′ from the other protomer. The B helices of either protomer interdigitate by matching Gly-75 where the helices cross each other. In addition to this interface, the carboxy terminal amino acids of both protomers wrap around one another allowing the carboxylate group of Gly-126 to salt bridge with Arg-119 from the other protomer. These protomer interactions form an extensive and common hydrophobic core in the context of the overall fold of the dimer. The substantial dimer interface occupies 4037.0 Å^2 of solvent accessible surface area per dimer compared with the total dimer surface area of 9610.3 Å^2 as calculated by GRASP (25) using a 1.4-Å probe radius.

Zinc Binding. PKCI-1 binds zinc with micromolar affinity (3, 5, 11). The protein structures of PKCI-1 were solved using crystals of zinc–PKCI-1, apo-PKCI-1, and an apo-PKCI-1 crystal into which 0.1 mM zinc acetate had been soaked. Zinc could not be detected in any of the three structures. Although there are obvious changes in the solubility and behavior of zinc–PKCI-1 in

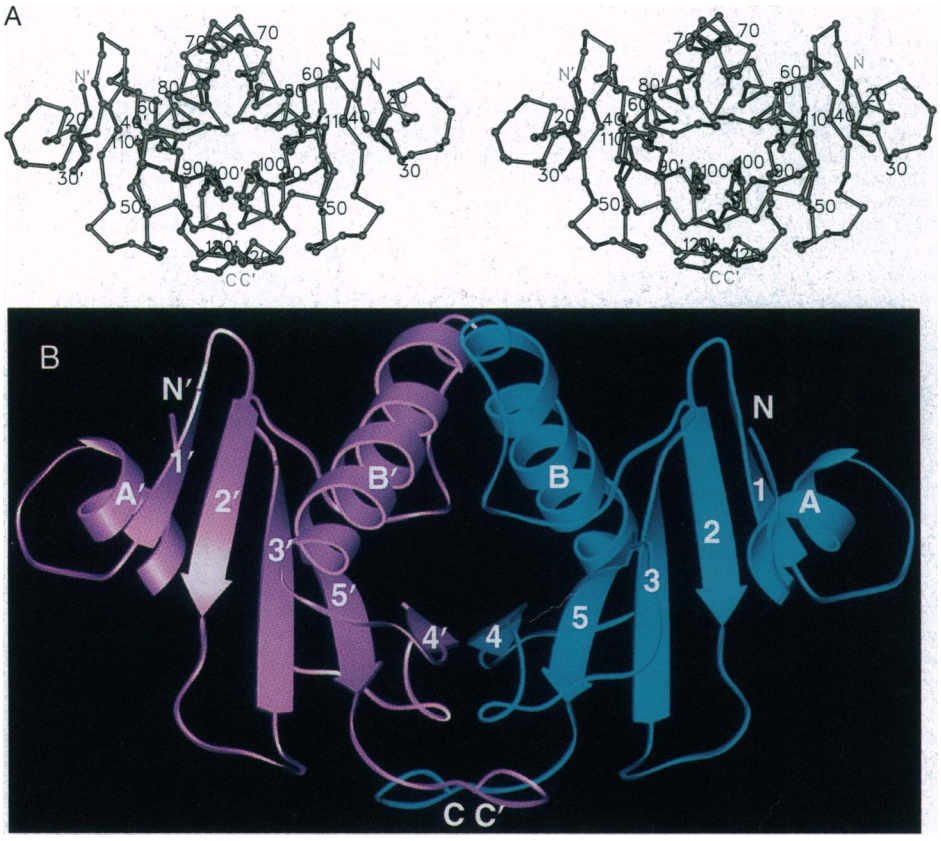

FIG. 2. (*A*) Stereo C$^\alpha$ backbone trace of PKCI-1 with C$^\alpha$ positions numbered every 10 amino acids. The numbering is differentiated between protomers by use of a prime symbol. (*B*) C$^\alpha$ spline Richardson ribbon diagram of PKCI-1 with helical elements lettered A (residues 18–23) and B (residues 71–86) and β elements numbered 1 (residues 31–35), 2 (residues 38–42), 3 (residues 50–56), 4 (residues 94–100), and 5 (residues 111–118). These figures were generated using SETOR (24).

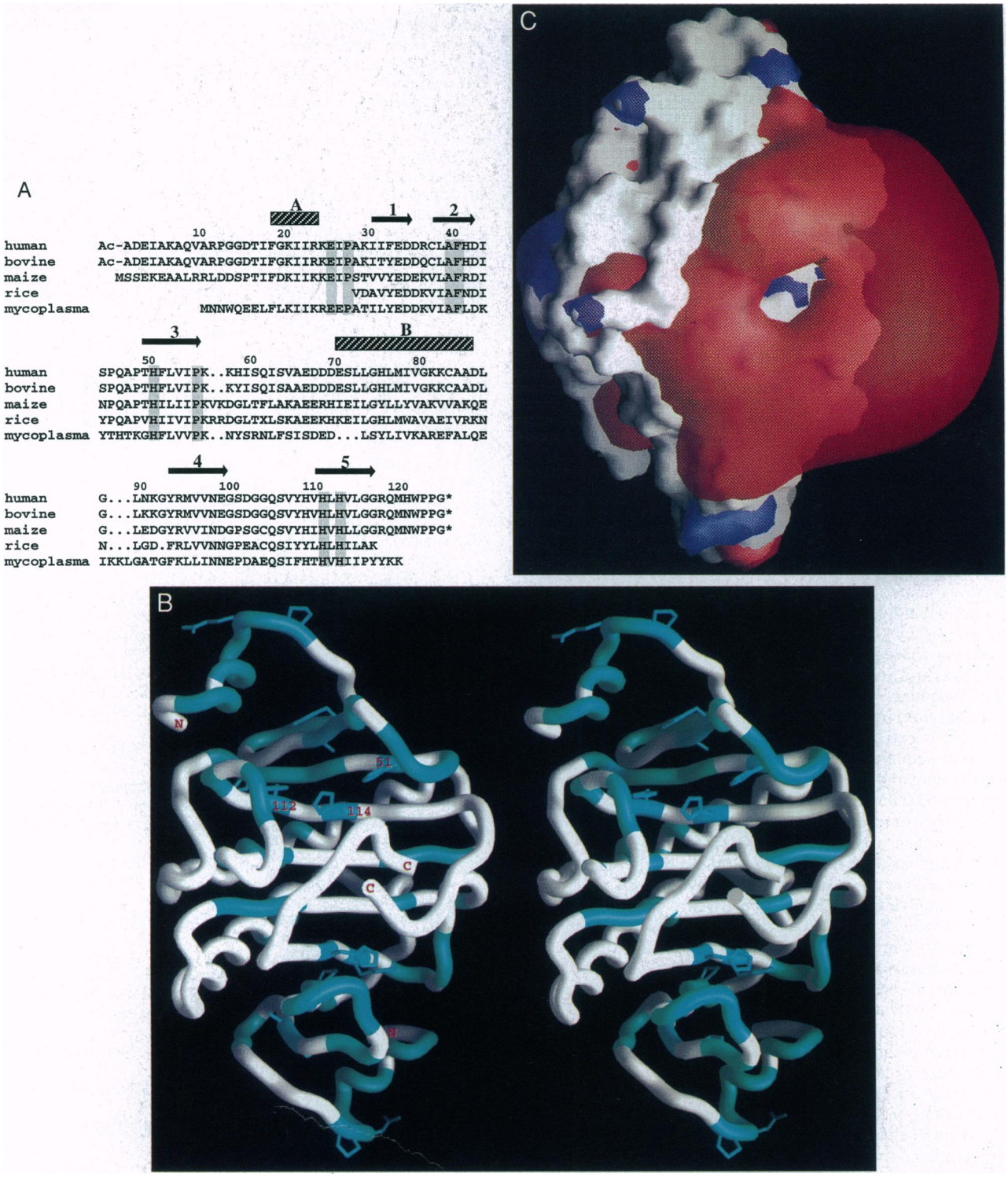

FIG. 3. (*A*) Amino acid sequence alignment of several representative PKCI-1 family members. Helical regions are denoted by a cross-hatched bar and β strands are denoted by bars with arrows over the aligned sequence. Secondary structural elements are numbered as in Fig. 2*B*. Residues completely conserved in all family members are highlighted in grey. (*B*) Stereo C^{α} spline generated by GRASP (25). Light blue regions of the C^{α} trace indicate identity in at least 8 of the 11 sequences of PKCI-1 family members aligned to date. Dark blue regions of C^{α} and side chains indicate residues that are completely conserved throughout the PKCI-1 family by sequence analysis. PKCI-1 sequences used for this alignment and structural analysis include those from *Homo sapiens*, *Bos taurus* (GenBank data base accession no. U09405), *Rattus norvegicus* (U09407), *Synechococcus sp.* (M34833), *Zea mays* (Z29643), *Brassica juncea* (U09406), *Plasmodium falciparum* (T18067), *Oryza sative callus* (D21291), *Azospirillum brasilense* (ABISHAFE), *Mycoplasma hyorhinis* (X14140), *Mycobacterium laprae* (U15187), and *Saccharomyces cerevisiae* (4). (*C*) Orthogonal view to *B* depicting the molecular surface of PKCI-1 and its electrostatic potential contoured at $\pm 2.5\ k_bT/e$ (k_bT being the product of the Boltzmann constant and the temperature, and e is the charge of an electron). Red depicts negative electrostatic potential and blue depicts the positive electrostatic potential. Acidic residues on the surface of PKCI-1 conserved in higher eukaryotes include residues 34–36 and 67–71. Acidic residues conserved through almost all organisms include 34–36, 67, and 68.

solution and in crystallization experiments, no structural manifestations of these properties can be detected. As such, we propose that the crystal structure of PKCI-1 determined in the presence of zinc is similar to the apo structure because the crystallization conditions act to force PKCI-1 into the apo conformation. Proteolysis experiments were done on the apo and

zinc forms of the protein using subtilisin. A protease-resistant form of PKCI-1 was formed by loss of the amino terminal nine amino acids. Truncated apo-PKCI-1 is stable over long periods of time in the presence of protease whereas truncated zinc–PKCI-1 is degraded over time without accumulation of other stable fragments as detectable by SDS/PAGE (C.D.L., unpublished observations). It has been observed before, namely by circular dichroism, that PKCI-1 exhibits a change in secondary structure over time in the presence of zinc (3, 5). Limited proteolysis of apo and zinc forms of the enzyme indicate that the zinc form of the protein is alternatively folded in comparison to apo-PKCI-1 and undergoes nonspecific degradation in the presence of a proteolytic enzyme, suggesting that zinc–PKCI-1 may adopt a conformation unlike that observed in our crystal structures.

Structural Basis for Zinc Binding. Analysis of the PKCI-1 structures and related sequences indicated that the residues involved in zinc binding may not be those initially identified by peptide mapping (3). We compared several protein sequences of PKCI-1 family members in light of our structural information. It became obvious that the histidyl residues poised to interact with zinc are most likely His-112, His-114, and His-51 in the structures reported here. His-110, a histidine initially thought to interact with zinc, is not completely conserved among family members and is not in a position where it could easily interact with His-112 and His-114. His-51 is completely conserved throughout the family and is proximal to His-112 and His-114 which are also completely conserved (Fig. 3*A*). The alternative folding suggested for zinc-PKCI-1 in solution could be explained by having His-51, His-112, and His-114 rearrange to bind zinc. It should be noted that many of the conserved residues surrounding the three histidines are hydrophobic in character and exposed to solvent.

Structural and Sequence Similarity in the PKCI-1 Family of Proteins. Sequence alignments between PKCI-1 family members ranging from mycoplasma to plants to humans reveal that this protein is extremely well conserved throughout nature. Amino acid sequence identity for the entire coding region between human and bovine PKCI-1 (94.4%), between human and maize (53.0%), and between human and mycoplasma PKCI-1 (30.6%) indicate that the structure of this protein is well conserved in a broad range of life forms (Fig. 3*A*). In addition, it appears that many of the residues on the surface of the protein are very well conserved throughout this range of organisms, implying that PKCI-1 may share common functional partners in all of these organisms (Fig. 3*B*). Although no distinct activity can be attributed to PKCI-1 at this time, it is intriguing to observe this level of identity in such a broad range of organisms. A possible common feature of PKCI-1 is the electrostatic distribution around the molecule (Figure 3c). Several conserved and exposed acidic residues on one face of the protein contribute to form a large negative electrostatic field. Although it has yet to be proven that these residues are important for PKCI-1 function *in vivo*, the asymmetry of charge distribution for the molecule is quite striking.

The structural elucidation of human PKCI-1 provides the first three-dimensional model for this ubiquitous family of proteins. Armed with this structural information, the search for functional roles for this protein *in vivo* can now be designed with precision.

Note. Recently a PKCI-1 homologue has been cloned from *Homo sapiens* as the putative tumor suppressor gene at locus 3p14.2, a region often homozygously deleted in many esophageal, stomach, and colon tumors and tumor-derived cell lines. This PKCI-1 homologue has been termed FHIT by Ohta *et al.* (26) The hypothetical translation product of FHIT has ≈50% identity to the *Schizosaccharomyces pombe* PKCI-1 homologue which has been shown to be a diadenosine 5′,5‴-P^1,P^4-tetraphosphate (Ap_4A) asymmetrical hydrolase by Robinson *et al.* (27), thus suggesting that FHIT is also an Ap_4A asymmetrical hydrolase. Human PKCI-1 is not an Ap_4A asymmetrical hydrolase; however, substrates have been identified for which human PKCI-1 exhibits hydrolytic activity (C.D.L., unpublished results). Although human PKCI-1 has only ≈25% identity with FHIT, the sequence identity corresponds with those regions highlighted in Figs. 3 *A* and *B*. The HIT family of proteins may therefore represent a structural superfamily in which FHIT and human PKCI-1 exist within separate functional subfamilies. It should be noted that the term HIT refers to the histidine triad near the carboxy terminus in this family (His-110, His-112, and His-114 in the human PKCI-1 sequence). Based on this structural analysis, His-51 should replace His-110 in this triad due to its proximity to His-112 and His-114. Protein Data Bank accession codes for the three refined structures are 1kpa (zinc protein), 1kpb (apo protein), and 1kpc (apo plus zinc protein). The GenBank accession code for human PKCI-1 is U51004.

We thank C. Ogata, H. Yamaguchi, and L. Shapiro for their help during data collection at beamline X4A; J. P. Lidestri for his help during data collection at Columbia University; and D. Fremont for his critical reading of this manuscript. This work was supported in part by a Helen Hay Whitney Foundation Fellowship to C.D.L., by National Institutes of Health Grant GM34102 to W.A.H., by National Cancer Institute Grant CA02656, and by an award from the Lucille Markey Charitable Trust to I.B.W.

1. MacDonald, J. R. & Walsh, M. P. (1985) *Biochem. J.* **232,** 559–567.
2. MacDonald, J. R., Groschel-Stewart, U. & Walsh, M. P. (1987) *Biochem. J.* **242,** 695–705.
3. Pearson, J. D., DeWald, D. B., Mathews, W. R., Mozier, N. M., Zurcher-Neely, H. A., Heinrikson, R. L., Morris, M. A., McCubbin, W. D., McDonald, J. R., Fraser, E. D., Vogel, H. J., Kay, C. M. & Walsh, M. P. (1990) *J. Biol. Chem.* **265,** 4583–4591.
4. Nishizuka, Y. (1984) *Nature (London)* **308,** 693–698.
5. Robinson, K., Jones, D., Howell, S., Soneji, Y., Martin, S. & Aitken, A. (1995) *Biochem. J.* **307,** 267–272.
6. Fraser, E. D. & Walsh, M. P. (1991) *FEBS Lett.* **294,** 285–289.
7. Brzoska, P. M., Chen, H., Zhu, Y., Levin, N. A., Disatnik, M.-H., Mochly-Rosen, D., Murnane, J. P. & Christman, M. F. (1995) *Proc. Natl. Acad. Sci. USA* **92,** 7824–7828.
8. Bustos, S., Schaefer, M. R. & Golden, S. S. (1990) *J. Bacteriol.* **172,** 1998- 2004.
9. Seraphin, B. (1992) *J. DNA Sequencing Mapping* **3,** 177–179.
10. Robinson, K. & Aitken, A. (1994) *Biochem. J.* **304,** 662–664.
11. Mozier, N. M., Walsh, M. P. & Pearson, J. D. (1991) *FEBS Lett.* **279,** 14–18.
12. Kahn, S. M., O'Driscoll, K. R., Jiang, W., Borner, C., Xu, D. B., Blackwood, M. A., Zhang, Y.-J., Nonoto, K. & Weinstein, I. B. (1994) *Carcinogenesis* **15,** 2919–2925.
13. Marmon, G. V. S., Wand, W. & Crabtree, G. R. (1994) *Science* **266,** 2002–2006.
14. Schowalter, D. & Sommer, S. (1989) *Anal. Biochem.* **177,** 90–94.
15. Jankarik, J. & Kim, S. H. (1991) *J. Appl. Crystallogr.* **24,** 409–411.
16. Otwinowski, Z. (1993) in *Data Collection and Processing*, eds. Sawyer, L., Isaacs, N. & Bailey, S. (SERC Daresbury Laboratory, Warrington, U.K.), pp. 56–62.
17. CCP4 SERC (UK) (1979) *Collaborative Computing Project 4* (Daresbury Laboratory, Warrington, U.K.).
18. Jones, T. A., Zou, J. Y., Cowan, S. W. & Kjeldgaard, M. (1991) *Acta Crystallogr. A* **47,** 110–119.
19. Brunger, A. T., Kuriyan, J. & Karplus, M. (1987) *Science* **235,** 458–460.
20. Brunger, A. T. (1992) *Nature (London)* **355,** 472–474.
21. Navaza, J. (1984) *Acta Crystallogr. A* **50,** 157–163.
22. Papov, V. V., Gravina, S. A., Mieyal, J. J. & Biemann, K. (1994) *Protein Sci.* **3,** 428–434.
23. Orengo, C. A. & Thornton, J. M. (1993) *Structure* **1,** 105–120.
24. Evans, S. V. (1993) *J. Mol. Graph.* **11,** 134–138.
25. Nicholls, A., Sharp, K. A. & Honig, B. H. (1987) *J. Comp. Chem.* **9,** 327–335.
26. Ohta, M., Inoue, H., Cotticelli, M. G., Kastury, K., Baffa, R., Palazzo, J., Siprashvili, Z., Mori, M., McCue, P., Druck, T., Croce, C. M. & Huebner, K. (1996) *Cell* **84,** 587–597.
27. Robinson, A. K., Pena, C. E. & Barnes, L. D. (1993) *Biochim. Biophys. Acta* **1161,** 139–148.